Solar Energy Materials & Solar Cells 161 (2017) 232–239

Contents lists available at ScienceDirect

Solar Energy Materials & Solar Cells

journal homepage: www.elsevier.com/locate/solmat

Improved environmental stability of highly conductive nominally undoped ZnO layers suitable for n-type windows in thin film solar cells

M. Hála[a,*], H. Kato[b], M. Algasinger[c], Y. Inoue[b], G. Rey[a], F. Werner[a], Ch. Schubbert[c], T. Dalibor[c], S. Siebentritt[a]

[a] Laboratory for Photovoltaics (LPV), Physics and Materials Science Research Unit, University of Luxembourg, 41 r. du Brill, L-4422 Belvaux, Luxembourg
[b] TDK Corporation Technical Center, 2-15-7, Higashi Owada, Ichikawa, Chiba 272-8558, Japan
[c] AVANCIS GmbH, Otto-Hahn-Ring 6, 81739 München, Germany

ARTICLE INFO

Keywords:
TCO
Zinc oxide
Photovoltaic devices
Thin films solar cells
Damp heat stability
Optoelectrical properties

ABSTRACT

Highly conductive nominally undoped ZnO (b-ZnO), obtained by means of an additional plasma near the substrate during sputter deposition, represent an attractive alternative for ZnO:Al (AZO) commonly employed in transparent windows of thin film solar cells. b-ZnO layers exhibit more than twice higher charge carrier mobility in comparison to AZO layers of the same resistivity ($1 \cdot 10^{-3}$ Ω cm). In consequence, a better transparency in near infrared region and an enhanced short circuit current can be achieved for low band gap thin film solar cells. Replacement of AZO for b-ZnO thus enhances their energy output.

In order to allow assessment of suitability of these b-ZnO films for deployment in photovoltaic industry, we examine their stability in various environments, and show pathways to improve it. We demonstrate that the b-ZnO films can exhibit comparable stability to ZnO:Al films in both ambient and heated air over the period of 24 months. However, the examined b-ZnO films degrade faster in accelerated open damp heat (DH) conditions, which we attribute to the lower compactness of columnar microstructure. In order to circumvent this limitation, we introduce a novel multilayered b-ZnO film with an improved environmental stability, as verified by the enhanced optoelectrical performance of DH-treated Cu(InGa)$(SSe)_2$ solar cells.

1. Introduction

1.1. ZnO layers with high near infrared transparency

Thin film solar cells have a substantially lower carbon footprint compared to the standard wafer technologies [1]. These solar cells rely on the upper-most transparent conductive oxide (TCO) layer which forms an n-type window. One way to improve the energy output of these solar cells is to increase the transparency of this window without compromising its conductivity.

TCO films based on ZnO are affordable alternatives to costly In_2O_3:Sn (ITO). The most common variation is Al-doped ZnO (AZO) that is highly conductive and highly transparent in the visible (VIS) spectral region [2,3]. However, AZO has a major drawback in the pronounced light absorption in the near infrared (NIR) spectral region, owing to the significant free carrier absorption caused by high concentration of free carriers. This is detrimental in those applications where NIR transparency is of importance. For instance, the use of AZO contact layer lowers the amount of light that can be used for effective energy conversion in thin film solar cells based on Cu(In,Ga)(SSe_2) and $Cu_2ZnSn(SSe)_4$ absorbers featuring low band gap, Eg ≤ 1.2 eV.

An alternative to AZO with comparably high conductivity but a better NIR transparency is nominally undoped ZnO [2,4–6] that can exhibit a significantly higher NIR transparency. This is related to a lower density of more mobile charge carriers which in the latter case originate in the variations in zinc/oxygen stoichiometry, or in the background doping by hydrogen [2,4,5].

Moreover, as in the case of AZO films, the highly conductive nominally undoped ZnO can be deposited by planar magnetron sputtering [4–7], which is a popular industrially-used technique that allows large area coating at low deposition temperatures (below 80 °C) required for solar cell stack fabrication.

The nominally undoped ZnO films with resistivities below $1 \cdot 10^{-3}$ Ω cm were recently prepared at ambient temperature by application of an additional plasma ignited by means of low-power RF substrate biasing during nonreactive sputtering from a ceramic ZnO target [6]. These layers, labelled as b-ZnO films (for biased ZnO), exhibit about 2.5 times lower charge carrier density in comparison to

* Corresponding author.
E-mail address: matej.hala@uni.lu (M. Hála).

http://dx.doi.org/10.1016/j.solmat.2016.11.015
Received 14 July 2016; Received in revised form 15 October 2016; Accepted 8 November 2016

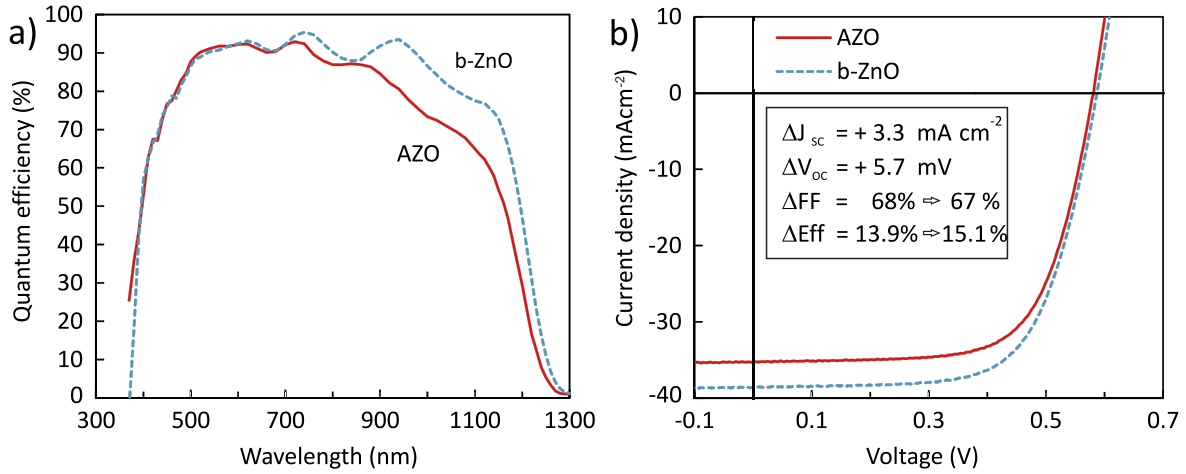

Fig. 1. External quantum efficiency spectra (a) and IV characteristics under irradiation (b) of the two solar cells with the TCO window formed by either an AZO layer (full line), or a b-ZnO layer (dashed line). These cells are prepared atop an identical Cu(In,Ga)(SSe_2) absorber. The enumerated increase or decrease of the principal solar cell characteristics due to the replacement of the AZO window for the b-ZnO window is summarized in the inset of (b).

the AZO films of identical resistivity. In consequence, their transparency in the NIR spectral region is significantly improved. A replacement of an AZO film by a b-ZnO film as the n-type window of low band gap chalcopyrite and kesterites thin film solar cells thus enhances their short circuit current [6].

The above claim is illustrated in Fig. 1 on the example of the spectral response and optoelectrical characteristics of the two solar cells fabricated from an identical Cu(In,Ga)(SSe_2) (CIGS) absorber (Eg=1 eV). It can be observed that the external quantum efficiency (EQE) spectra of the solar cell finished with a b-ZnO window shows a substantially higher amplitude in NIR region (i.e., for $\lambda > 750$ nm), if compared to its counterpart with an AZO window (Fig. 1a). This results in the rise of the respective short circuit current density, J_{SC}, by +3.3 mA cm^{-2}, as depicted in Fig. 1b. It is to be noted that the higher J_{SC} is also translated into an improved power conversion efficiency, Eff, from 13.9% to 15.1% (+9%), despite a slightly lowered fill factor, FF (−1%). The open circuit voltage, V_{OC}, is not significantly affected (< + 1%).

1.2. Stability issue of ZnO-based layers

An important prerequisite of TCO for its application in thin film solar cell modules is the inherent damp heat (DH) stability. It is known that the sputtered AZO used in commercial CIGS thin film modules protected by encapsulation (with lamination foil, edge sealing and cover glass) does not limit the DH stability of those modules. It is thus of crucial importance that the new TCO material does also not compromise module stability, in order to avoid higher requirements for the encapsulation.

The commonly observed conductivity drop of the ZnO-based layers exposed to DH conditions can be explained on one hand by the inherent instability of ZnO material in the presence of water that is either the source of the degradation process (e.g., hydrolysis reactions) or, at least, a catalyst of the physical or chemical processes [8,9]. On the other hand, the columnar microstructure exhibited by all the polycrystalline ZnO films grown from vapor phase [10,11] features columnar boundaries that represent possible pathways for penetration of water and other reactive agents deep into the film [9,12,13].

It has been also reported that the water in-diffusion within ZnO films is specifically pronounced if these layers are less compact, for instance, as a consequence of their growths at elevated Ar pressures [12] or atop rough substrates (e.g., CIGS absorbers), in which case the microstructure exhibits extended grain boundaries [13]. In fact, the water vapors can get adsorbed at the exposed film surface and then diffuse within the film through accessible columnar and grain boundaries [8,9,13]. The adsorbed water molecules and their products (e.g., formed hydroxides) are believed to act as electron traps, resulting in the accumulation of trapped electrons at the grain boundaries. This raises the potential barrier that the free electrons have to overcome [14], and thus increases their cross-boundary scattering.

The studies cited above are with no exception related to the environmental stability of extrinsically doped ZnO (mostly AZO), while the stability of the nominally undoped ZnO is rather unexplored; It is commonly reported that nominally undoped ZnO films are prone to degrade faster than AZO films even at relatively low (e.g., ambient) temperatures [2,3,7], specifically if they are prepared by post-deposition treatment (e.g., by H plasma exposure [2] or UV illumination [15]).

In contrary to these reports, recent work indicated that the b-ZnO films made conductive due to RF substrate biasing can possess an excellent stability in ambient air, and only a slightly lower high temperature stability than AZO films [6]. However, it is the resistance of b-ZnO films to harsh conditions (e.g., in damp heat) that can be decisive for their application as the n-type windows in photovoltaic industry.

1.3. Scope of this work

The motivation of the current work is to seek the answers for the following three questions;

1. How the stability of b-ZnO compares to that of AZO?
2. Is the degradation mechanism of b-ZnO films in harsh environments comparable to that of doped ZnO films?
3. What are the means of improving b-ZnO films' stability?

In particular, we investigate the stability of the b-ZnO films tested in various environments. These include ambient air, heated air at 105 °C, as well as the accelerated ageing in DH conditions using 95 °C and 85% humidity. For rigorous assessment of the damp heat stability, both films and completed solar cell stacks are tested in DH with no encapsulation (open DH). Afterwards, we attempt to relate the obtained findings to the crystallographic characteristics of the films under investigation, and suggest pathways for improvements. Finally, we demonstrate a multilayered b-ZnO coating with enhanced DH resistance.

2. Experimental details

The TCO depositions were performed in a commercial semi-

automated sputtering deposition system equipped with 7.5 cm diameter ceramic ZnO and AZO (2 wt% of Al_2O_3) targets powered by an RF generator in non-reactive Ar atmosphere using a pressure of 0.13 Pa (1 mTorr). In the deposition of ZnO and b-ZnO films the power load at the target was fixed to 125 W, and in the deposition of AZO films to 140 W. The substrates, soda lime glass or partial solar cell stacks (prepared by AVANCIS), were positioned at a distance of 13 cm on an unheated substrate holder that was optionally biased by an additional RF generator. In b-ZnO film depositions, the self-induced negative DC voltage on the RF-powered substrate holder, referred to as RF bias voltage U_b, was assured by the application of an RF signal to the substrate holder, employing low power densities (i.e., below 0.01 W cm^{-2}). U_b was fixed to 25 V during growth of all single layer b-ZnO films, but it was varied in the range from 25 V to 100 V in the preparation of multilayered b-ZnO films.

The film thickness of each TCO sample was measured with a profilometer, and the corresponding resistivity ρ was determined using a homebuilt four point probe setup in Van-der-Pauw configuration [16]. Hall mobility μ_{Hall} and free carrier density n_e were evaluated using Hall measurements performed also in Van-der-Pauw configuration, at a magnetic field of 0.57 T (AVANCIS), and in a wide range of magnetic fields up to 7 T (University of Luxembourg).

The optical properties were analyzed with a spectrophotometer; Transmittance ($T(\lambda)$) and reflectance ($R(\lambda)$) were measured and fitted with the formulae in Reference [17] in order to retrieve the complex refractive index spectra. The corresponding near infrared dielectric constant spectra were subsequently fitted using the Drude model [18,19] in order to enumerate the plasma wavelength, and to derive the optical mobility, μ_{opt}, using n_e previously estimated by Hall analysis.

The crystallinity of the TCO films was investigated by X-Ray diffractometry (XRD) in $\theta - 2\theta$ and θ-rocking curve (RC) geometries using the Cu Kα radiation. The X-ray coherence length, d_{XRD}, was enumerated from the broadening of the $\theta - 2\theta$ ZnO 002 diffraction peak using Scherrer formula [20], and the c lattice parameter size, c_{XRD}, was evaluated from the position of the $\theta - 2\theta$ ZnO 002 diffraction peak. The crystallite alignment was estimated using the broadening full width at half maximum (FWHM) of the ZnO 002 diffraction peak obtained in the RC geometry. The morphology of the selected coatings was analyzed by cross-sectional scanning electron microscopy (SEM) using Hitatchi SU-70.

Cu(In,Ga)(SSe_2) (CIGS) absorbers were fabricated by AVANCIS R & D baseline, using the stacked elemental layer rapid thermal (SEL-RTP) process [21].

The current-voltage (IV) behaviour of the completed solar cell devices was then evaluated in a commercial 1-sun simulator in order to extract J_{SC}, V_{OC}, FF and Eff characteristics. Their external quantum efficiency (EQE) was also evaluated in the wavelength range of 300–1300 nm.

The accelerated ageing in open damp heat (DH) was executed in a dedicated environmental chamber using 95 °C (10 °C more than prescribed by the standard environmental test IEC 61646) and 85% relative humidity.

3. Results and discussion

3.1. Ambient air ageing

The ambient stability of b-ZnO films deposited on flat soda lime glass (SLG) substrates was investigated by monitoring their resistivity, ρ, during a long period of ambient air exposure (i.e., room conditions), and compared to that of a reference AZO film.

Fig. 2a depicts that the resistivity of the AZO films does not change significantly (increases by less then 2% during 24 months of air exposure). Instead, the resistivity of the b-ZnO films of various thickness (280–520 nm) analyzed during the same period of time slightly increases, by 4% (b-ZnO 420 nm) to 16%. Even thinner b-ZnO films (than the ones presented here) that were exposed to ambient air during 32 months exhibited a resistivity rise $\Delta\rho \leq +3 \cdot 10^{-4}\ \Omega$ cm (not shown). The above observations reveal good ambient air stability of all the (unencapsulated) b-ZnO layers under investigation; it is to be stressed that such a small increase in film resistivity would not affect thin film solar cell performance.

In Fig. 2a it can be seen that an occasional drop in b-ZnO film resistivity that further lowers the corresponding $\Delta\rho$ is observed. The reason for this unexpected behaviour is not yet understood, as the previously assumed correlation with the season of the year [6] was not confirmed. However, one can speculate that the actual air humidity during the resistivity analyses may be of importance since the drop in $\Delta\rho$ is higher for thinner or more degraded samples that can exhibit a rougher surface; this effect is also witnessed by the pronounced drop in ρ of the ZnO 520 nm film after 22 months of anneling, as visible in Fig. 2b.

3.2. Dry heat ageing

In the second set of experiments the resistivity of b-ZnO and reference AZO films on the SLG substrates was monitored during their annealing in an oven filled with air at 105 °C. The humidity within the oven was not controlled, but it is reasonable to assume that it can reach a few %. Humidity-induced degradation thus can't be excluded, even though it has to be significantly less pronounced than in the DH conditions. It is to be stressed that the resistivity was always analyzed at the ambient temperature.

The resistivity of thin b-ZnO films (thickness below 400 nm) was found to rise exponentially as suggested by the respective marks in Fig. 2b. A steeper resistivity rise indicates an increasing rate of heat-induced degradation with decreasing film thickness. In order to understand the reason for this relation, XRD analyses have been performed on the b-ZnO layers under investigation, using the samples that were aged in the ambient air.

An example of a diffractogram obtained using $\theta - 2\theta$ geometry from a b-ZnO film which depicts the ZnO 002 diffraction peak employed in all the XRD analyses is illustrated in Fig. 2 in Ref. [22]. The broadening of the $\theta - 2\theta$ ZnO 002 diffraction peaks suggested that the thinner b-ZnO films possess a lower X-Ray coherence length, d_{XRD}, as also depicted here in the legend of Fig. 2a.

Similar observations of smaller d_{XRD} (and a higher in-plane mechanical stress) with decreasing layer thickness were previously reported also for both ZnO and AZO [23]. A lower d_{XRD} indicates a smaller average distance between structural defects in the perpendicular direction to the substrate surface. In addition, it was found that the thinner b-ZnO films exhibit a larger FWHM of the θ-rocking curve (RC) ZnO 002 diffraction peak, suggesting a lower order of grain alignment (results not shown).

The above findings are of no surprise since the columnar structure of ZnO exhibited by all AZO and b-ZnO films (as verified by cross-sectional SEM) possess significantly smaller cystallographic features (e.g., smaller grain size and columnar width) and a lower texture degree closer to the underlying substrate as a consequence of limited growth dynamics at temperatures far from thermal equilibrium [11,24]. In consequence, thinner films are expected to feature a higher amount of lattice defects such as open columnar boundaries also at the layer's surface. These crystalline imperfections represent possible pathways to any air-carried reactive agents (e.g., H_2O and CO_2) that may diffuse into the film, facilitated by the elevated temperature, get adsorbed at the grain boundaries (e.g., in a form of hydroxides and carbonates), and negatively affect charge carrier transport as discussed in the introduction. Similar observations of compromised DH stability was previously reported for thinner AZO films [12,13].

The relation of the film crystallinity and the dry heat ageing stability is also supported by the characteristics of the 420 nm thick b-ZnO film highlighted by empty circles in Fig. 2. It is to be stressed that the

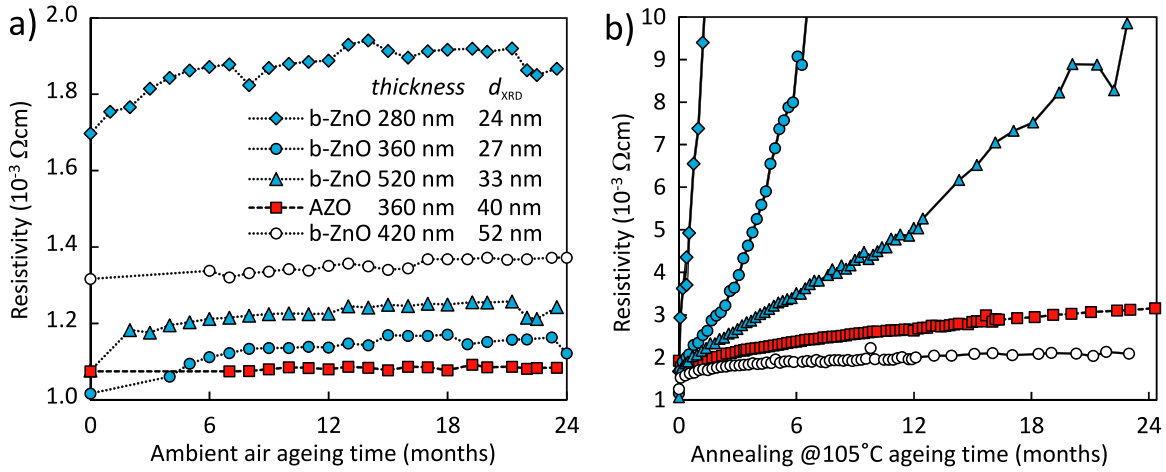

Fig. 2. Film resistivity as a function of time during 24 months of exposure to either the ambient air (a), or to the air kept at 105 °C (b) for b-ZnO layers of various thickness (diamond, circle and triangle marks) and for a reference AZO layer (square marks). Film's thicknesses and X-ray coherence lengths, d_{XRD}, are identified in (a).

resistance of this b-ZnO film was found to rise slower during 24 months of annealing ($\Delta\rho \approx +9{\cdot}10^{-4}$ Ω cm, Fig. 2b) than that of the 100 nm thicker b-ZnO film, and even slower than that of the reference AZO layer of similar thickness (AZO 360 nm). The same b-ZnO 420 nm film also exhibits the best ambient air stability from all the b-ZnO films, as witnessed by the lowest resistivity rise during 24 month-long ambient air ageing ($\Delta\rho \approx +0.6{\cdot}10^{-4}$ Ωcm, Fig. 2a).

The $\theta - 2\theta$ XRD analyses performed on this b-ZnO 420 nm film revealed that the ZnO 002 diffraction peak possesses a significantly higher intensity than observed from any other b-ZnO film prepared in our laboratory (not shown), suggesting an enhanced crystallinity. The other examined XRD characteristics do also indicate such conclusion; d_{XRD} is substantially larger (52 nm), and the FWHM of the ZnO 002 diffraction peak from the XRD θ-rocking curve analyses is significantly smaller (4.1°), than are the corresponding d_{XRD} and FWHM values obtained from all the reference samples of 370–390 nm thickness, as summarized in Fig. 3.

Moreover, in Fig. 3 it can be seen that the c_{XRD} lattice parameter of the b-ZnO 420 nm film is lower than c_{XRD} of the other b-ZnO films. Since the c_{XRD} closer to the value expected for the unconstrained ZnO crystals (c_{bulk} = 5.207 Å [25])) indicates a lower in-plane lattice strain, the latter observation suggests a lower level of residual compressive stress within the b-ZnO 420 nm film.

It can thus be concluded that this particular b-ZnO 420 nm film has a substantially improved crystallinity compared to the other b-ZnO films under investigation and also to the AZO films of comparable thickness. A lower amount of structural imperfections may then hinder the penetration of air-carried reactive substances into the film, and thus improve its stability.

Based on the findings of the environmental tests depicted in Fig. 2 and on the results of the crystallographic analyses presented in Fig. 3, it can be stated that the b-ZnO films prepared under the optimized deposition conditions can exhibit comparable ambient and heat stability as the standard AZO films. However, these conditions are yet to be defined, as the outstanding environmental resistance of the b-ZnO 420 nm film could not be reproduced in the successive deposition experiments.

Finally, it is to be noted that we did not observe any effect of substrate composition on the dry heat stability of b-ZnO and AZO layers, as tested in dry heat experiments employing films prepared onto both SLG (containing Na and other chemical elements) and quartz (no additives) substrates using identical deposition conditions; The respective resistivity rise during 20 months of dry heat ageing was not affected by the substrate type (results not shown).

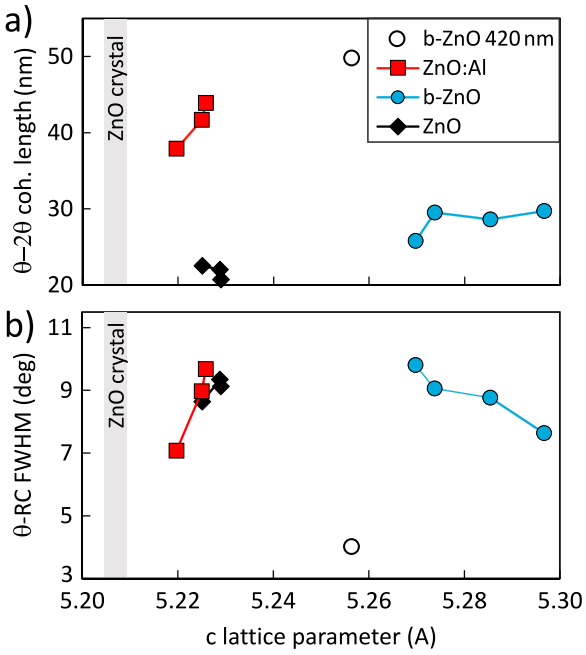

Fig. 3. XRD $\theta - 2\theta$ coherence length (a) and XRD θ-rocking curve (RC) FWHM (b) of the ZnO 002 diffraction peak as a function of c_{XRD} lattice parameter of several ZnO-based films of comparable thickness (370–400 nm), namely AZO films (square marks), b-ZnO films (filled circle marks) and ZnO films (diamond marks), and of the b-ZnO 420 nm film (empty circle mark). c_{bulk} value for an unconstrained ZnO crystal [25] is also depicted. It is to be noted that all the films were prepared using comparable deposition conditions, but over the period spanning up to 24 months.

3.3. Open damp heat ageing

Accelerated ageing in open DH conditions during a week period was performed on the two pairs of b-ZnO and AZO layers of different thickness range (360 and 370 nm, and 850 and 830 nm, respectively). These four n-type window representatives were prepared onto bare SLG substrates, and characterized prior open DH exposure.

Afterwards, they were regularly removed from the DH chamber for film resistivity and Hall analyses (for ρ, μ_{Hall} and n_e determination), of which results are shown in Fig. 4a–c. In addition, the transmittance and reflectance spectra ($T(\lambda)$ and $R(\lambda)$) of both bilayers were acquired prior and after the accelerated ageing experiments for the purpose of optical mobility evaluation from the plasma wavelength (the μ_{opt} values corresponding to the thicker pair of b-ZnO and AZO layers are noted in the inset of Fig. 4b).

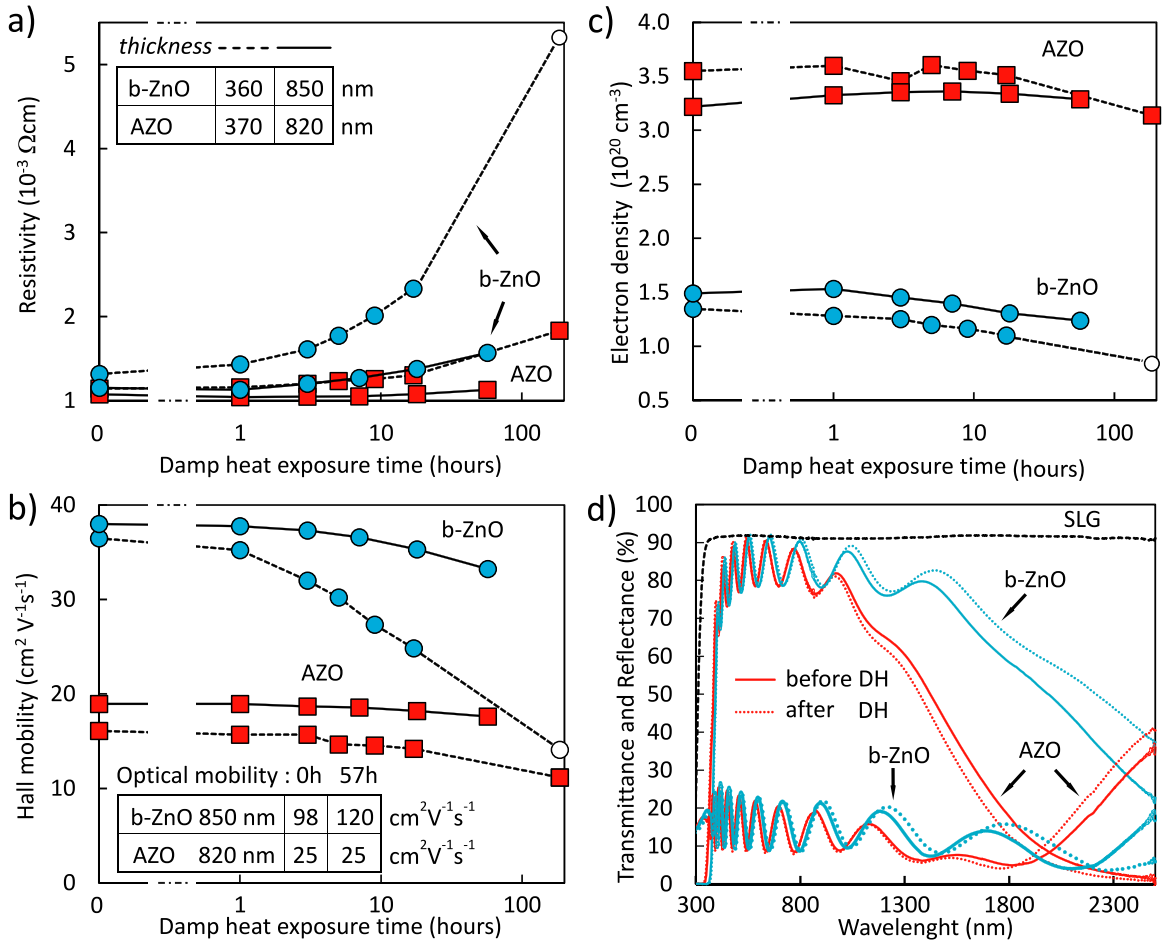

Fig. 4. The evolution of film resistivity (a), electron Hall mobility (b), and electron density (c) of b-ZnO (circle marks) and AZO (square marks) films of two different thickness ranges (specified in the inset of (a)), as a function of accelerated open DH exposure (in log scale). The empty symbols stand for the Hall analyses performed at the University of Luxembourg and the filled symbols for those performed at AVANCIS. Optical mobility μ_{opt} evaluated for the thicker pair of TCO layers is in the inset of (b). (d) Optical transmittance (higher curves) and reflectance (lower curves) spectra of the b-ZnO 850 nm and AZO 820 nm layers deposited on the SLG substrates evaluated before (in solid lines) and after (in dashed lines) a week of accelerated ageing in open DH conditions.

One should note that the as-deposited b-ZnO films of 360 nm and 850 nm thickness exhibit approximately 2.2 times higher electron mobility μ_e (at 0 h in Fig. 4b) and about 2.4 times lower electron density n_e (Fig. 4c), in comparison to their AZO counterparts of the same thickness. It is due to the lower n_e that the 850 nm thick b-ZnO film depicted in Fig. 4d has also a significantly higher transmittance and a lower reflectance in the NIR spectral region.

Fig. 4a illustrates that a week-long accelerated DH ageing causes an increase in ρ by approximately 300% and 50% for b-ZnO 360 nm and b-ZnO 850 nm films, respectively, in contrast to the comparably thick AZO films for which much lower rise in ρ is observed (by +63% for AZO 370 nm and by +5% for AZO 820 nm). The increase in ρ in all four cases can be related mostly to the decrease in Hall mobility; The values of μ_{Hall} drop by about −70% and −12% for the b-ZnO films, and by −30% and −7%, for the AZO films (Fig. 4b). The electron density decreases as well, by −30% and −17% for b-ZnO films, and by −12% for the AZO 370 nm film (Fig. 4c). (Instead, n_e for AZO 850 nm increases by up to +4% after several hours of DH ageing, and then starts dropping. The reason for this phenomenon is not understood). Fig. 4d also shows that there are no changes in the VIS transparency for both of the films, while a significant rise in the NIR transmittance of the b-ZnO layer reflects the reduced carrier density within DH-treated b-ZnO 850 nm film.

If compared to μ_{Hall} values, the optical mobility obtained from the Drude model using $T(\lambda)$ and $R(\lambda)$ analyses of the two thicker layers (summarized in Fig. 4b) follow distinctively different trends; μ_{opt} of b-ZnO 850 nm film increased from 98 to 120 $cm^2 V^{-1} s^{-1}$ (in consequence of the increased average time between two successive scattering events of free electrons), while μ_{opt} of the AZO 820 nm film does not change.

μ_{Hall} that decreases at a higher rate than μ_{opt} suggests a deterioration of free electron transport across grain boundaries, as demonstrated on the example of comparably thick AZO films grown on both smooths and rough substrates [13]. However, in the case of b-ZnO 850 nm film the trends in μ_{Hall} (decreasing) and μ_{opt} (rising) are even opposite. This indicates that the respective electron transport driven by an electric field is hampered by a rising grain boundary scattering, the same way as in DH-treated AZO films. This suggests that the mechanism of b-ZnO films' degradation can mostly be related to the density of the crystallographic imperfections (such as an average grain size and columnar width) that are inherent to the columnar microstructure, rather than to (in)stability of b-ZnO doping.

It is to be stressed that the density of grain boundaries and other lattice imperfections is supposed to be substantially higher in both of the investigated b-ZnO films in comparison to the AZO films. This is suggested by the d_{XRD} data plotted in Fig. 3a, indicating that all the studied 370–400 nm thick b-ZnO layers possess a substantially smaller average distance between structural defects than comparably thick AZO layers ($d_{XRD} \approx 29$ nm for b-ZnO in comparison to $d_{XRD} \approx 41$ nm for AZO). A significant difference in d_{XRD} was also observed in the case of the two thicker layers tested by DH ageing ($d_{XRD} = 42$ nm for b-ZnO 850 nm film and $d_{XRD} = 52$ nm for AZO 820 nm film, not shown).

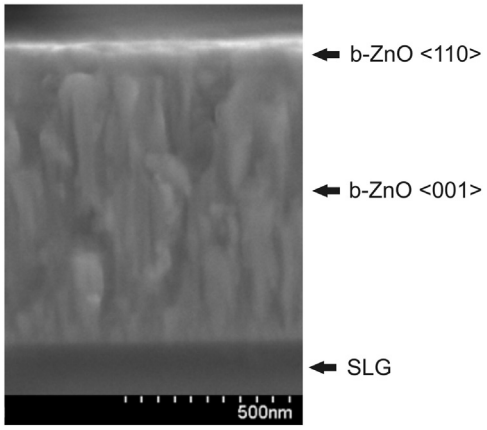

Fig. 5. The cross-sectional SEM image of the 770 nm thick b-ZnO multilayer coating consisting of a b-ZnO ⟨001⟩ base layer covered by a thin b-ZnO ⟨110⟩ overlayer.

Taking the assumption that the d_{XRD} values are at least rough indicatives of the volume density of grain boundaries and other lattice faults, it is rather expectable that the environmental stability of the investigated b-ZnO films is lower than that of the reference AZO films.

3.4. Pathways towards stable b-ZnO films: multilayered b-ZnO

Following the same logic as above, it can be stated that the b-ZnO films can be made more stable in harsh environments if the density of lattice imperfections that allow in-diffusion of detrimental species is lowered. In other words, if their microstructure would be more compact. An example of such a film is the highy stable ZnO 420 nm (d_{XRD} = 52 nm) discussed in Section 3.2. It is not unreasonable to assume that its open DH stability would outperform the b-ZnO 360 nm film and that it could even compete with the AZO 370 nm film (dashed lines in Fig. 4).

It is hard to trace what the origin for the improved crystallinity of the b-ZnO 420 nm film was. However, one may speculate that it may be related to the higher plasma density during that particular deposition process (for a reason that is not known). A higher plasma density above the growing film kept at a low-voltage bias (e.g., U_b = 25 V used in the current study) would cause a higher influx of plasma-generated charged species (e.g., Ar ions). Such low-energy ion bombardment delivers an additional energy to the condensing adatoms that can be used for their enhanced surface diffusion allowing to reach the most convenient binding position atop the under-lying surface. This is known to be highly beneficial for densification of the microstructure of both polycrystalline [26] and amorphous [27] films grown from a vapor phase at low deposition temperatures. It is thus suggested that the exposure of growing films to denser plasma densities in combination of low-voltage biasing might be one of the pathways towards more compact b-ZnO films of enhanced environmental stability.

Another approach how to increase the resistance of the b-ZnO films against harsh environments is to make the open columnar boundaries and other crystallographic imperfections less accessible to aggresive substances. It has been proposed [28], that this can be assured by a multilayered coating featuring a thicker b-ZnO film covered by a (thinner) overlayer comprising at least one b-ZnO film of different crystallographic texture. As the upper film is forced to re-nucleate and to develop its own textured columns atop the underlying layer, it will cover the columnar boundaries of the latter. It can thus be expected that such “cover” will act as a less permeable barrier that imposes a more complex path (in terms of in-diffusion) for water or any other reactive agents discussed previously. The film texture can also be altered, in order to obtain multiple interfaces that would reinforce the barrier effect.

It is to be stressed that a strong polar ⟨001⟩ texture is commonly observed for the ZnO and AZO films reported in literature, and also for all the films reported in this study so far, including the b-ZnO films. The modification of the prevalent ⟨001⟩ texture can be achieved during a unique deposition process by changing the RF bias amplitude; Both non-polar ⟨110⟩ and ⟨101⟩ textures can be reached if a certain RF bias threshold is reached [29], or if the RF bias amplitude is not kept steady but varied in a continous matter [28].

The latter approach was applied in preparation of two prototypes of multilayered films that comprised a 770 nm thick b-ZnO layer (with ⟨001⟩ texture) covered by a 70 nm thick b-ZnO overlayer (with ⟨110⟩ texture). More specifically, the driving RF power (and thus the U_b value) was cycled from U_b = 25 V to U_b = 100 V and back in a repetitive manner (with 60 s ramping time). One of the overlayers was made using 14 ramping cycles with no pauses in between, while the other one employed only 5 ramping cycles and 120 s pauses at each of the two U_b extremities.

The reason for this biasing pattern is to induce a stronger ⟨110⟩ texture within the overlayer. The presence of the < 110 > texture was verified in a separate experiment in which another 380 nm thick b-ZnO film, prepared at the identical deposition conditions as the 70 nm overlayer, exhibited a more pronounced 110 reflection peak than b-ZnO films prepared using a steady RF bias amplitude (e.g., U_b = 100 V). Here, it should be stressed that the b-ZnO ⟨110⟩ coating deposited atop an SLG substrate does not exhibit a better environmental resistance than b-ZnO ⟨001⟩ films of comparable thickness, as also tested by dry heat ageing (results not shown).

Fig. 5 shows the morphology of the first of the two b-ZnO multilayer prototypes in which both the b-ZnO ⟨001⟩ base layer and the b-ZnO ⟨110⟩ overlayer (prepared using 14 cycles of RF bias variation) are identified. It can be seen that the columnar width in the base layer visibly enlarges with a rising distance from the SLG substrate, while the columns within the overlayer are much thinner and hardly discernable (also for the poor quality of the SEM image). This is a clear sign that this latter layer grew from new nucleation centers atop the underlying thicker one. It is to be underlined, that the optoelectrical properties of this b-ZnO stack are not significantly compromised by the overlayer presence [28], while its environmental stability is substantially improved. This is witnessed by the dry heat ageing experiments [22], and by the open DH analyses of unencapsulated solar cells equipped with the b-ZnO multilayers that are discussed in the next section.

3.5. Open damp heat ageing of CIGS solar cells

In order to rigorously assess the environmental stability of the b-ZnO films applicable as transparent conductive window contacts atop functional solar cell devices, it is crucial to investigate their optoelectrical performance in open DH conditions if covering rough substrates (such as are the large-grain CIGS absorbers) [13]. For this reason, partial CIGS solar cell stack (AVANCIS) processed up to the i-ZnO layer in the AVANCIS R & D baseline in Munich have been transferred to the University of Luxembourg and equipped with either an AZO layer, a b-ZnO layer, or with one of the two b-ZnO multilayer prototypes discussed in the last section. The total thickness of these n-type windows was approximately 850 nm.

The four types of layered stacks were finished into functioning solar cell devices by mechanical scribing into numerous solar cells (16 cells for each sample), and by contacting the front of the solar cells with e-beam evaporated metals. All the solar cells were then analyzed by current-voltage (IV) characterization in order to test their performance.

The average values of the power conversion efficiency, fill factor, J_{SC} and V_{OC}, evaluated from the IV curves of the 8 centrally-positioned solar cells during the incremental amount of hours of open DH exposure, are depicted in Fig. 6, accompanied by the enumerated drop of the averaged values due to the 57 h of open DH treatment (within the inset of each graph). For clarity reasons, only the results related to the b-ZnO multilayer prototype depicted in Fig. 5 (labelled as b-ZnO

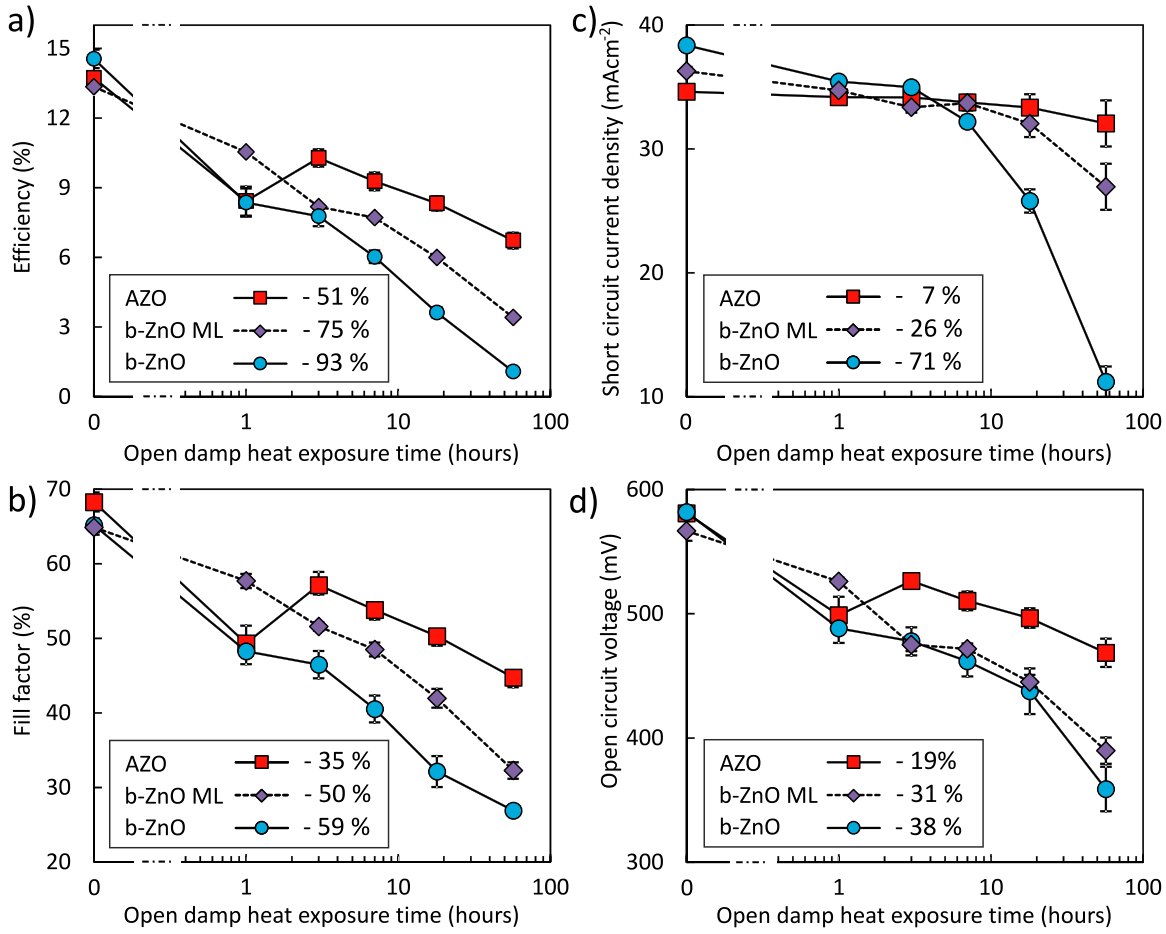

Fig. 6. The power conversion efficiency (a), fill factor (b), shortcircuit current density (c) and open circuit voltage (d) analyzed from the set of 8 model solar cells as a function of accelerated open DH exposure (in log scale). The solar cells were coated by transparent contact film comprising either a standard AZO layer, a single layer of b-ZnO, or a multilayer b-ZnO coating (b-ZnO ML, depicted in Fig. 5) featuring a 70 nm thick b-ZnO of different texture. The relative average drop in the examined solar cell characteristics due to the 57 h of exposure to the open DH conditions is also summarized in the inset of each figure.

ML) are displayed in Fig. 6, since the second prototype exhibited similar trends in all characteristics.

The accelerated ageing in open DH creates significantly harsher test conditions than are those commonly employed in the photovoltaic industry. In consequence, the average optoelectrical characteristics of even the most resistant solar cells in this investigation, the cells featuring the reference AZO film, exhibit a significant deterioration; After the 57 h of open DH exposure the conversion efficiency decreases by −51%, the FF value by ΔFF = −35%, J_{SC} by $\Delta J_{SC} = -7\%$, and V_{OC} by $\Delta V_{OC} = -19\%$.

The solar cells equipped with a single layer b-ZnO film exhibit even substantially larger decrease in all the monitored characteristics. This may be related to the largest drop in FF (ΔFF = −59%); The final value of FF = 27% indicates that the devices do not show diode IV characteristics anymore. The origin for the diode quality deterioration might be the modified recombination paths of charge carriers within the space charge region, and/or the increasing influence of parasitic resistances. Both of these effects that are difficult to be disentangled may be fingerprints of the deteriorating b-ZnO films' microstructure due to penetrating water vapors, as discussed in Section 3.3.

Fig. 6 also shows that the optoelectrical characteristics of the solar cells equipped with the b-ZnO ML prototype decrease in their amplitude at much lower rate than those of the cells coated with the single layer b-ZnO. In particular, the solar cells coated with b-ZnO ML exhibit ΔFF = −50% and $\Delta J_{SC} = -26\%$. In consequence, the respective conversion efficiency after the 57 h of ageing in the open DH is in average 3 times higher (with a drop of −75%) than that of the solar cells equipped with the standard b-ZnO film. This observation confirms the enhanced DH stability of the b-ZnO ML prototype, which thus serves as a proof of concept that the multilayered b-ZnO coatings offer an enhanced environmental stability. Further improvements are expected if a proper optimization of the deposition procedure is undertaken.

4. Conclusions

This work demonstrates that the highly conductive and transparent b-ZnO films with an improved NIR transparency can compete with the standard AZO films in terms of their stability in the ambient as well as in the heated air. Their ambient air stability tested over the period of 24 months is comparable to that of the reference AZO film, and a b-ZnO film with an improved crystallinity showed even better stability in dry heat ageing. However, the specimen of the b-ZnO films aged in open DH conditions exhibited faster degradation than the AZO films, as indicated by a more pronounced drop in both charge carrier density and Hall mobility, and by the compromised optoelectrical characteristics of the CIGS solar cells coated with the corresponding n-type windows.

Furthermore, it was found that b-ZnO films prepared under the non-optimized deposition conditions (with respect to the exceptionally resistant b-ZnO layer with significantly improved crystallinity) exhibit smaller X-ray coherence length than AZO films, suggesting a lower compactness of the columnar microstructure. This permits an easier in-diffusion of water and/or other reactive substances, which in turn raises grain boundary scattering of free electrons, as also suggested by

decreasing Hall mobility but not-decreasing optical mobility. Degradation of b-ZnO films can thus be more related to their compactness, rather than to the stability of doping.

In order to overcome the compromised stability of the examined b-ZnO films due to the limitations imposed by the lower crystalline compactness of the columnar microstructure, prototype multilayered b-ZnO windows featuring a 70 nm b-ZnO overlayer of different texture were tested atop unencapsulated CIGS-based solar cells. The respective solar cells exhibited substantially lower deterioration of all the monitored optoelectrical characteristics if compared to those solar cells equipped with a single layer b-ZnO film, suggesting thus the reduced in-diffusion of detrimental agents.

Acknowledgment

The authors wish to thank Mr. Thomas Schuler (Universtity of Luxembourg) for his expert technical assistance, Dr. Michele Melchiorre (Universtity of Luxembourg) for SEM analyses, Dr. Yves Flemming (Luxembourg Institute of Science and Technology, LIST) for his patient assistance with rocking curve XRD analyses, and LIST for the access to the XRD and profilometry equipment. The financial support of TDK Corporation within the NOTO Project is gratefully acknowledged.

References

[1] M. de Wild-Scholten, V. Cassagne, T. Huld, Solar resources and carbon footprint of photovoltaic power in different regions in Europe, in: Proc. 29th Eur. Photovoltaic Sol. Energy Conf. (Amsterdam, Netherlands), 2014, p. 3421.

[2] K. Ellmer, Electrical properties, in: K. Ellmer, A. Klein, B. Rech (Eds.), Transparent Conductive Zinc Oxide: Basics and Applications in Thin Film Solar Cells, Springer, Berlin, 2008, pp. 34–78.

[3] A.E. Delahoy, S. Guo, Transparent conducting oxides for photovoltaics, in: A. Luque, S. Hegedus (Eds.), Handbook of Photovoltaic Science and Engineering, John Wiley & Sons, Ltd, Chichester, 2011, pp. 716–796. http://dx.doi.org/10.1002/9780470974704.ch17.

[4] D.K. Murti, Substrate biased RF sputtering of zinc oxide films, Appl. Surf. Sci. 11/12 (1982) 308–314. http://dx.doi.org/10.1016/0378-5963(82)90077-0.

[5] H. Nanto, T. Minami, S. Shooji, S. Takata, Electrical and optical properties of zinc oxide thin films prepared by rf magnetron sputtering for transparent electrode applications, J. Appl. Phys. 55 (4) (1984) 1029–1034. http://dx.doi.org/10.1063/1.333196.

[6] M. Hála, S. Fujii, A. Redinger, Y. Inoue, G. Rey, M. Thevenin, V. Deprédurand, T.P. Weiss, T. Bertram, S. Siebentritt, Highly conductive ZnO films with high near infrared transparency, Prog. Photovolt: Res. Appl. 23 (11) (2015) 1630–1641. http://dx.doi.org/10.1002/pip.2601.

[7] S. Maniv, C.J. Miner, W.D. Westwood, Transparent conducting zinc oxide and indium-tin oxide films prepared by modified reactive planar magnetron sputtering, J. Vac. Sci. Technol. A 1 (3) (1983) 1370–1375. http://dx.doi.org/10.1116/1.572024.

[8] F.J. Pern, R. Noufi, B. To, C. DeHart, X. Li, S.H. Glick, Degradation of ZnO-based window layers for thin-film CIGS by accelerated stress exposures, in: Proc. SPIE 7048 7048, 2008, 70480P. ⟨http://dx.doi.org/10.1117/12.795097⟩.

[9] J. Hüpkes, J. Owen, M. Wimmer, F. Ruske, D. Greiner, R. Klenk, U. Zastrow, J. Hotovy, Damp heat stable doped zinc oxide films, Thin Solid Films 555 (2014) 48–52. http://dx.doi.org/10.1016/j.tsf.2013.08.011.

[10] F.C.M. van de Pol, F.R. Blom, T.J.A. Popma, R.f. planar magnetron sputtered ZnO films I: structural properties, Thin Solid Films 204 (2) (1991) 349–364. http://dx.doi.org/10.1016/0040-6090(91)90074-8.

[11] Y. Kajikawa, Texture development of non-epitaxial polycrystalline ZnO films, J. Crys Growth 289 (1) (2006) 387–394. http://dx.doi.org/10.1016/j.jcrysgro.2005.11.089.

[12] T. Tohsophon, J. Hüpkes, S. Calnan, W. Reetz, B. Rech, W. Beyer, N. Sirikulrat, Damp heat stability and annealing behavior of aluminum doped zinc oxide films prepared by magnetron sputtering, Thin Solid Films 511–512 (2006) 673–677. http://dx.doi.org/10.1016/j.tsf.2005.12.130.

[13] D. Greiner, N. Papathanasiou, A. Pflug, F. Ruske, R. Klenk, Influence of damp heat on the optical and electrical properties of Al-doped zinc oxide, Thin Solid Films 517 (7) (2009) 2291–2294. http://dx.doi.org/10.1016/j.tsf.2008.10.107.

[14] J.Y.W. Seto, The electrical properties of polycrystalline silicon films, J. Appl. Phys. 46 (12) (1975) 5247–5254. http://dx.doi.org/10.1063/1.321593.

[15] A. Illiberi, F. Grob, C. Frijters, P. Poodt, R. Ramachandra, H. Winands, M. Simor, P.J. Bolt, High rate (7 nm/s), atmospheric pressure deposition of ZnO front electrode for Cu(In,Ga)Se_2 thin-film solar cells with efficiency beyond 15%, Prog. Photovolt.: Res. Appl. 21 (8) (2013) 1559–1566. http://dx.doi.org/10.1002/pip.2423.

[16] L.J. van der Pauw, A method of measuring the resistivity and hall coefficient on lamellae of arbitrary shape Philips Tech. Rev. 20, (8), 1858/59, pp. 220–224.

[17] E.N. Kotlikov, G.V. Tereshchenko, Study of optical constants of films used for the synthesis of broad-band antireflection coatings, Opt. Spectrosc. 82 (1997) 603–609.

[18] N.W. Ashcroft, N.D. Mermin, Solid State Physics, Saunders College Publishing, 1976.

[19] G. Rey, C. Ternon, M. Modreanu, X. Mescot, V. Consonni, D. Bellet, Electron scattering mechanisms in fluorine-doped SnO_2 thin films, J. Appl. Phys. 114 (18) (2013) 183713. http://dx.doi.org/10.1063/1.4829672.

[20] J.I. Langford, A.J.C. Wilson, Scherrer after sixty years: a survey and some new results in the determination of crystallite size, J. Appl. Crystallogr. 11 (2) (1978) 102–113. http://dx.doi.org/10.1107/S0021889878012844.

[21] J. Palm, V. Probst, F.H. Karg, Second generation CIS solar modules, Sol. Energy 77 (6) (2004) 757–765. http://dx.doi.org/10.1016/j.solener.2004.05.011.

[22] M. Hála, Y. Inoue, H. Kato, G. Rey, F. Werner, C. Schubbert, M. Algasinger, T. Dalibor, S. Siebentritt, Environmental stability of highly conductive nominally undoped ZnO layers, in: Proc. 43rd IEEE Photovoltaic Spec. Conf., Portland, OR, 2016, pp. 1–5, (in press).

[23] R. Cebulla, R. Wendt, K. Ellmer, Al-doped zinc oxide films deposited by simultaneous rf and dc excitation of a magnetron plasma: relationships between plasma parameters and structural and electrical film properties, J. Appl. Phys. 83 (2) (1998) 1087–1095. http://dx.doi.org/10.1063/1.366798.

[24] J.A. Thornton, Influence of apparatus geometry and deposition conditions on the structure and topography of thick sputtered coatings, J. Vac. Sci. Technol. 11 (4) (1974) 666–670. http://dx.doi.org/10.1116/1.1312732.

[25] K. Ellmer, A. Klein, ZnO and its applications, in: K. Ellmer, A. Klein, B. Rech (Eds.), Transparent Conductive Zinc Oxide: Basics and Applications in Thin Film Solar Cells, Springer, Berlin, 2008, pp. 1–33.

[26] I. Petrov, P.B. Barna, L. Hultman, J.E. Greene, Microstructural evolution during film growth, J. Vac. Sci. Technol. A 21 (5) (2003) S117–S128. http://dx.doi.org/10.1116/1.1601610.

[27] M. Hála, R. Vernhes, O. Zabeida, E. Bousser, J. Klemberg-Sapieha, R. Sargent, L. Martinu, Growth and properties of high index Ta_2O_5 optical coatings prepared by HiPIMS and other methods, Surf. Coat. Technol. 241 (0), 2014, pp. 33–37, Selected Papers from the Society of Vacuum Coaters 56th Annual Technical Conference – SVC TechCon 2013. ⟨http://dx.doi.org/10.1016/j.surfcoat.2013.08.024⟩.

[28] M. Hála, P. Dale, S. Siebentritt, Transparent conducting film based on zinc oxide, LU 93080.

[29] S. Takayanagi, T. Yanagitani, M. Matsukawa, Y. Watanabe, A simple technique for obtaining (1120) or (1010) textured ZnO films by RF bias sputtering, in: Proceedings of IEEE Int. Ultrason. Symp., 2010, pp. 1060–1063. http://dx.doi.org/10.1109/ULTSYM.2010.5935655.